A. Colagrossi, V. Pesce, L. Bucci, F. Colombi, M. Lavagna
Guidance, Navigation and Control for 6DOF Rendezvous in Cislunar Multi-Body Environment
Aerospace Science and Technology, Vol. 114, 2021, 106751 (16 pages)
doi:10.1016/j.ast.2021.106751

Guidance, navigation and control for 6DOF rendezvous in Cislunar multi-body environment

Andrea Colagrossi[a,1,*], Vincenzo Pesce[a,1], Lorenzo Bucci[a,2], Francesco Colombi[a,3], Michèle Lavagna[a,4]

[a] *Department of Aerospace Science and Technology, Politecnico di Milano, Via La Masa 34, 20156, Milano, Italy*

---

[*] Corresponding author

Email addresses: `andrea.colagrossi@polimi.it` (Andrea Colagrossi), `vincenzo.pesce@polimi.it` (Vincenzo Pesce), `lorenzo.bucci@polimi.it` (Lorenzo Bucci), `francesco.colombi@mail.polimi.it` (Francesco Colombi), `michelle.lavagna@polimi.it` (Michèle Lavagna)

[1] Postdoctoral Research Fellow.

[2] Ph.D. Candidate.

[3] M.Sc. Student.

[4] Full Professor.

Abstract

Recent studies highlighted the benefits of a support infrastructure located in Cislunar environment, which would ease the design of forthcoming space missions with a favorable access from and to the lunar surface, the Earth and many interplanetary destinations. Multi-body orbits rose a peculiar interest and were selected to stage a human-robotic exploration outpost; the family of Near Rectilinear Halo Orbits (NRHO), in particular, appears specifically suitable in these regards. Among the different capabilities that such outpost will tend to, the docking with other crewed or autonomous vehicles is a key feature that shall be present. Although low Earth orbit (LEO) rendezvous and docking is well assessed, no mission has performed such task in a multi-body gravitational environment. The paper presents a guidance, navigation and control (GNC) framework for 6 degrees of freedom (6DOF) coupled Cislunar rendezvous and docking. A feasible operational rendezvous scenario is detailed and exploited to define open-loop and closed-loop GNC functions for far-range and close-range. Then, the final approach is analyzed, proposing a closed-loop GNC that encompasses coupled translational-rotational dynamics. Vision-based only relative navigation techniques are applied to Cislunar multi-body dynamics to guarantee a coupled state estimation with a simple suite of sensors and a broad applicability range, ranging from passively cooperative to non-cooperative or unknown target spacecraft.

Keywords

Cislunar Space; Multi-body Orbit; Rendezvous; Guidance, Navigation and Control; Coupled 6DOF Dynamics.

1. Introduction

The Cislunar environment is a promising location for future space exploration architectures, both crewed and robotic. Recent studies and the Global

Exploration Roadmap [1, 2] highlighted the benefits of a support infrastructure located in such an environment, leveraging the dynamical features offered by non-Keplerian multi-body orbits. Among those, the family of Near Rectilinear Halo Orbits (NRHO), in particular, appears specifically suitable to stage a human-robotic exploration outpost [3].

The on-orbit operations of a complex and, possibly, modular space system in lunar vicinity would require a sound improvement in the available techniques to perform autonomous rendezvous and docking between uncrewed spacecraft in such peculiar space environment. In fact, although low Earth orbit (LEO) rendezvous and docking is well assessed by international space agencies, no mission has performed such task in a multi-body gravitational environment. Moreover, despite non-Keplerian n-body dynamics is well known and exploited in trajectory design and optimization studies [4], its application in Guidance, Navigation and Control (GNC) systems is more recent and occasionally overlooked in certain implementations [5]. As a matter of fact, supported by the idea of frequent updates in the navigation measurements, the GNC design may be sometimes founded on simple, albeit improper, 2-body based dynamical models. Rendezvous and docking operations require to consider also the rotational state of the spacecraft involved. Thus, the exploitation of coupled 6 degrees of freedom (6DOF) dynamics may be beneficial to design a comprehensive GNC chain, which is able to manage both the translation and rotation relative motion. In these regards, the inclusion of coupled attitude dynamics in multi-body Cislunar space environment is recent and not often included in GNC applications.

Existing literature provides different research studies dedicated to relative motion and rendezvous problem in Cislunar space. In 1971, Gerding formulated rendezvous equations in the vicinity of the second libration point of the Earth-Moon system [6]. Then, the study of relative dynamics control in the restricted 3-body problem was applied to formation flying by Gurfil [7] and Héritier [8]. More investigations about dynamical models and GNC strategies to support the design of rendezvous operations in Earth-Moon L2 orbits were presented by Mand, Sanchez and D'Souza [9, 10, 11]. Many of these works were developed on classic restricted 3-body formulations, which are helpful for a theoretical insight, but sometime lack a factual GNC implementation and an accurate dynamical modeling of Cislunar environment.

First studies about coupled 6DOF dynamics in multi-body orbits assumed the spacecraft as artificially maintained close to the equilibrium points and only the stability of the motion was considered by Kane [12] and Robinson [13]. In the second decade of the 21st century, the coupling between orbital and attitude motion was investigated by Guzzetti [14, 15], Colagrossi [16] and Bucci [17] providing different families of orbit-attitude solutions in restricted 3-body problem. The knowledge of orbit-attitude coupling in multi-body Cislunar space was applied to relative dynamics problems just in recent years [18], but a coupled 6DOF GNC framework has not yet proposed for this kind of scenario.

Relative navigation architectures strongly depend on the distances between the spacecraft involved in proximity operations. Above a few thousand meters, the usage of optical navigation techniques is limited to very coarse estimation of the line-of-sight; here, the attitude relative navigation is neither feasible nor relevant, since the attitude of the involved spacecraft will likely not be constrained for what concern the relative pose. On the contrary, when the proximity operations occur at a few hundred meters, optical techniques show promising results for relative 6DOF navigation [19]. These navigation approaches would not require additional sensors other than the optical ones, and they were proposed in recent years, by Zhang [20] and Pesce [21, 22], for generic orbits, not set in Cislunar space. Relative navigation for rendezvous in Cislunar multi-body environment was studied by Muñoz [23], who proposed different sensor fusion strategies to cope with the problem requirements. However, a 6DOF vision-based only navigation method is not available in existing non-Keplerian multi-body literature.

For these reasons, the paper presents a GNC framework to deal with the problem of 6DOF rendezvous in multi-body Cislunar environment, proposing guidance strategies, vision-based navigation techniques and control laws for a full orbit-attitude rendezvous and docking. The study is particularly keen on exploring the dynamical features of non-Keplerian environment in lunar vicinity, both to highlight the beneficial influence on the rendezvous design capabilities and to stress the limitations of GNC systems based on incorrect dynamical modeling. The GNC design, based on open-loop guidance at far-range and closed-loop guidance at close-range, is motivated by the relative trajectories trying to exploit the dynamical features of multi-body Cislunar orbits, both for maneuver cost minimization and for trajectory safety. Moreover, vision-based only navigation techniques are considered to prove the feasibility of this navigation method when applied to Cislunar environment; they are embedded in the proposed coupled 6DOF GNC architecture, when dealing with closed-loop guidance and control, while the spacecraft are in close proximity. This choice is beneficial for the whole GNC design, since it guarantees the largest applicability range of the presented methods, even with passively cooperative, non-cooperative or unknown spacecraft, or when a limited suite of sensors is available.

The resulting GNC formulation is motivated by a careful dynamical comparison among different modeling approaches, which is dedicated to highlight the large errors that are present whenever the actual non-Keplerian multi-body dynamics is neglected. The increased modelling complexity with respect to 2-body based dynamical models is justified with the reduction of the GNC update frequency, which is possible by exploiting the proper dynamics existing in Cislunar space.

Finally, a feasible rendezvous strategy is defined, analyzing the concept of the rendezvous operations with a passively cooperative vehicle in lunar NRHO.

2. Dynamical Models and Background

Cislunar space dynamics can be described exploiting a restricted n-body problem modeling approach, which considers the body T, with mass m_T, under the influence of the Earth, with mass m_E, and the Moon, with mass m_M, assuming $m_T \ll m_E, m_M$. The perturbations of Cislunar space, mainly due to

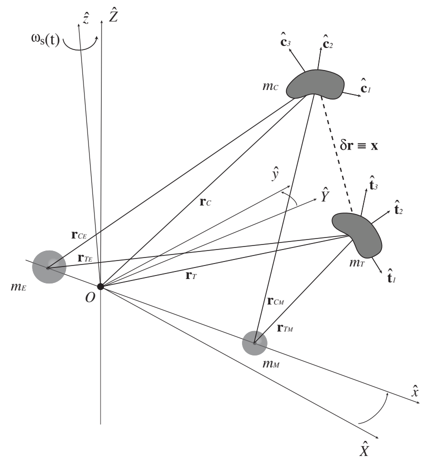

Figure 1: Absolute and relative 6DOF dynamics model.

the presence of the Sun and to the real motion of Earth and Moon, are included in the following discussion.

The body m_T is extended and three-dimensional, as represented in Figure 1. The position of its center of mass is described by the position vector $\mathbf{r}_T$, and the orientation of the body reference frame T with respect to an inertial reference frame, I, is conveniently described using the four-dimensional quaternion vector, ${}^I\mathbf{q}^T$, which represents a rotation from T to I. The frame I is centered at the center of mass of the system, O and it is defined by the axes $\hat{\mathbf{X}}$, $\hat{\mathbf{Y}}$ and $\hat{\mathbf{Z}}$.

The dynamics can also be conveniently visualized in a rotating reference frame, S, which is called Synodic frame. It is centered in O; the first axis, $\hat{\mathbf{x}}$, is aligned with the vector from m_E to m_M; the third axis, $\hat{\mathbf{z}}$, is in the direction of the angular velocity of S, $\boldsymbol{\omega}_S(t) = \omega_S(t)\hat{\mathbf{z}}$; $\hat{\mathbf{y}}$ completes the right-handed triad, as shown in Figure 1. It shall be noted that no assumption on circular motion of the two primaries has been done. Thus, the angular velocity of the Synodic frame is not constant in time, but it is defined by the actual motion of the Earth and the Moon around their common barycenter. At time $t = 0$, the rotating frame S is aligned to the inertial frame I and, in this paper, it is mainly used for visualization purposes.

2.1. Absolute Dynamics for 6DOF Rendezvous in Multi-body Orbits

The orbital equations of motion of the body m_T in Cislunar space can be written considering the gravitational attraction of the two primaries, plus the contribution of the Solar Radiation Pressure (SRP) and the fourth body gravity of the Sun acting on the Earth-Moon system [24]. The resulting absolute dynamics equations in the I frame are written in scalar form as:

$$\mathbf{f}_x = \begin{cases} \dot{x} = v_x \\ \dot{y} = v_x \\ \dot{z} = v_z \end{cases} \tag{1}$$

$$\mathbf{f}_v = \begin{cases} \dot{v}_x = -\frac{\mu_E(x-x_E)}{r^3_{T_E}} - \frac{\mu_M(x-x_M)}{r^3_{T_M}} + a_{SRP_x} + a_{4th_x} \\ \dot{v}_y = -\frac{\mu_E(y-y_E)}{r^3_{T_E}} - \frac{\mu_M(y-y_M)}{r^3_{T_M}} + a_{SRP_y} + a_{4th_y} \\ \dot{v}_z = -\frac{\mu_E(z-z_E)}{r^3_{T_E}} - \frac{\mu_M(z-z_M)}{r^3_{T_M}} + a_{SRP_z} + a_{4th_z}, \end{cases} \tag{2}$$

where x, y and z are the Cartesian coordinates of T expressed in terms of the Inertial reference frame, I; v_x, v_y and v_z are the velocity components of the body m_T in I; $a_{SRP_{x,y,z}}$ and $a_{4th_{x,y,z}}$ are the scalar components of the perturbing accelerations due to the SRP and to the gravitational effect of the Sun on the Earth-Moon system. The distances between the center of mass of m_T and the two primaries are respectively $r_{T_E} = \sqrt{(x-x_E)^2 + (y-y_E)^2 + (z-z_E)^2}$ for the Earth, and $r_{T_M} = \sqrt{(x-x_M)^2 + (y-y_M)^2 + (z-z_M)^2}$ for the Moon. The position vector of Earth, $\mathbf{r}_E = [x_E, y_E, z_E]^{\mathrm{T}}$, and Moon, $\mathbf{r}_M = [x_M, y_M, z_M]^{\mathrm{T}}$ are retrieved from their ephemerides. The standard gravitational parameters of Earth and Moon are indicated as $\mu_E = G\, m_E$ and $\mu_M = G\, m_M$, where G is the universal gravitational constant.

The attitude dynamics of the body m_T is described by the Euler equations of motion in Cislunar space [16]. Euler equations include the gravity torques exerted by the two primaries, the gravity gradient of the fourth body and the angular accelerations due to the Solar Radiation Pressure. The resulting Euler dynamical equations for the attitude dynamics are expressed as:

$$\mathbf{f}_\omega = \begin{cases} \dot{\omega}_1 = \frac{I_3 - I_2}{I_1}\left(\frac{3\mu_E}{r_{T_E}^5} l_2 l_3 + \frac{3\mu_M}{r_{T_M}^5} h_2 h_3 - \omega_2\omega_3\right) + \quad \alpha_{SRP_1} + \alpha_{4th_1} \\ \dot{\omega}_2 = \frac{I_1 - I_3}{I_2}\left(\frac{3\mu_E}{r_{T_E}^5} l_1 l_3 + \frac{3\mu_M}{r_{T_M}^5} h_1 h_3 - \omega_1\omega_3\right) + \quad \alpha_{SRP_2} + \alpha_{4th_2} \\ \dot{\omega}_3 = \frac{I_2 - I_1}{I_3}\left(\frac{3\mu_E}{r_{T_E}^5} l_1 l_2 + \frac{3\mu_M}{r_{T_M}^5} h_1 h_2 - \omega_1\omega_2\right) + \quad \alpha_{SRP_3} + \alpha_{4th_3}, \end{cases} \tag{3}$$

where ω_1, ω_2 and ω_3 are components of the angular velocity of the body relative to I and expressed in the body-fixed reference frame T, ${}^I\boldsymbol{\omega}^T$; l_i are the direction cosines in the reference T of the unit position vector from m_E to m_T, $\hat{\mathbf{r}}_{T_E}$; h_i are those related with $\hat{\mathbf{r}}_{T_M}$; $\alpha_{SRP_{1,2,3}}$ and $\alpha_{4th_{1,2,3}}$ are the components of the angular accelerations introduced before, respectively due to the SRP and to the gravitational influence of the Sun. I_1, I_2 and I_3 are the principal moments of inertia of m_T, $\mathbb{I}_T$.

The fundamental rules of attitude kinematics allow the propagation of the rotational motion from the attitude dynamics. In fact, it is possible to evaluate the time rate of change of the quaternion vector from the body angular velocity as:

$$\mathbf{f}_q = \begin{cases} \dot{q}_1 = \frac{1}{2}(\omega_1 q_4 - \omega_2 q_3 + \omega_3 q_2) \\ \dot{q}_2 = \frac{1}{2}(\omega_1 q_3 + \omega_2 q_4 - \omega_3 q_1) \\ \dot{q}_3 = \frac{1}{2}(-\omega_1 q_2 + \omega_2 q_1 + \omega_3 q_4) \\ \dot{q}_4 = -\frac{1}{2}(\omega_1 q_1 + \omega_2 q_2 + \omega_3 q_3), \end{cases} \tag{4}$$

where q_1, q_2, q_3 and q_4 are the quaternion components of ${}^I\mathbf{q}^T$.

2.2. Relative Dynamics for 6DOF Rendezvous in Multi-body Orbits

Relative dynamics in multi-body orbits is based on the absolute dynamics presented in the previous section. The formulation is developed for two bodies, target spacecraft, T, and chaser spacecraft, C, of generic masses m_T and m_C in the inertial reference frame I.

The relative translational dynamics is immediately available from the definition of the relative position vector, $\mathbf{x}$:

$$\mathbf{x} \equiv \delta\mathbf{r} = \mathbf{r}_C - \mathbf{r}_T, \tag{5}$$

which, in the inertial reference frame, can be straightforwardly differentiated in time obtaining:

$$\ddot{\mathbf{x}} = \ddot{\mathbf{r}}_C - \ddot{\mathbf{r}}_T, \tag{6}$$

where $\ddot{\mathbf{r}}_C$ and $\ddot{\mathbf{r}}_T$ are the absolute acceleration vectors of chaser and target (i.e. the reference), available from the absolute dynamics equations of the two bodies, in Equation (2). The inertial reference frame is convenient to derive the relative orbital dynamics since it allows having a direct comparison between relative and absolute trajectories, which is helpful to develop the GNC functions, as explained in Section 3.

The derivation of relative attitude dynamics is not straightforward as the translational one. In fact, it describes the rotational motion of the chaser relative to the target frame, or vice versa; in both cases, the relative attitude dynamics is expressed with respect to a non-inertial reference frame. In this research work, the relative attitude dynamics of the chaser with respect to the target is formulated in the body-fixed frame of the chaser, C.

The relative attitude dynamics formulation requires the introduction of a relative quaternion, $\delta\mathbf{q}$, representing the body-fixed frame of the chaser, C, with respect to the body-fixed frame of the target, T, which is defined as:

$$\delta\mathbf{q} = {}^I\mathbf{q}^C \times \left({}^I\mathbf{q}^T\right)^{-1} = \begin{bmatrix} \boldsymbol{\chi}\left({}^I\mathbf{q}^T\right)\ {}^I\mathbf{q}^C \\ \\ \left({}^I\mathbf{q}^T\right)^{\mathrm{T}}\ {}^I\mathbf{q}^C \end{bmatrix}, \tag{7}$$

where the matrix $\boldsymbol{\chi}({}^I\mathbf{q}^T)$ is a 3×4 matrix defined as:

$$\boldsymbol{\chi}({}^I\mathbf{q}^T) = \begin{bmatrix} q_{T_4}\mathbf{I}_{3\times3} - [\mathbf{q}_{T_{123}}\times] & -\mathbf{q}_{T_{123}} \end{bmatrix}. \tag{8}$$

In the previous equation, $\mathbf{q}_{T_{123}} = [q_{T_1}, q_{T_2}, q_{T_3}]^{\mathrm{T}}$ is the column vector part of the target quaternion, ${}^I\mathbf{q}^T$, and q_{T_4} is its scalar part; $\mathbf{I}_{3\times3}$ is the 3×3 identity matrix; $[\mathbf{q}_{T_{123}}\times]$ is the 3×3 skew-symmetric cross-product matrix. The rotation matrix $\mathbf{R}$, which transforms a vector from the target reference frame, T, to the chaser reference frame, C, can be expressed in terms of the relative quaternion,

$\delta \mathbf{q}$, as:

$$\mathbf{R}(\delta\mathbf{q}) = \begin{bmatrix} \delta\mathbf{q}_1^2 - \delta\mathbf{q}_2^2 - \delta\mathbf{q}_3^2 + \delta\mathbf{q}_4^2 & 2(\delta\mathbf{q}_1\delta\mathbf{q}_2 - \delta\mathbf{q}_3\delta\mathbf{q}_4) & 2(\delta\mathbf{q}_1\delta\mathbf{q}_3 + \delta\mathbf{q}_2\delta\mathbf{q}_4) \\ 2(\delta\mathbf{q}_1\delta\mathbf{q}_2 + \delta\mathbf{q}_3\delta\mathbf{q}_4) & -\delta\mathbf{q}_1^2 + \delta\mathbf{q}_2^2 - \delta\mathbf{q}_3^2 + \delta\mathbf{q}_4^2 & 2(\delta\mathbf{q}_2\delta\mathbf{q}_3 - \delta\mathbf{q}_1\delta\mathbf{q}_4) \\ 2(\delta\mathbf{q}_1\delta\mathbf{q}_3 - \delta\mathbf{q}_2\delta\mathbf{q}_4) & 2(\delta\mathbf{q}_2\delta\mathbf{q}_3 + \delta\mathbf{q}_1\delta\mathbf{q}_4) & -\delta\mathbf{q}_1^2 - \delta\mathbf{q}_2^2 + \delta\mathbf{q}_3^2 + \delta\mathbf{q}_4^2 \end{bmatrix}. \tag{9}$$

At this point, the relative angular velocity can be defined in I as:

$$\delta\boldsymbol{\omega}_I = \left({}^I\boldsymbol{\omega}^C\right)_I - \left({}^I\boldsymbol{\omega}^T\right)_I = {}^I\mathbf{A}^C \left(\left({}^I\boldsymbol{\omega}^C\right)_C - \mathbf{R}\left({}^I\boldsymbol{\omega}^T\right)_T\right), \tag{10}$$

where ${}^I\mathbf{A}^C = \left({}^C\mathbf{A}^I\right)^{\mathrm{T}}$ is the attitude matrix from the chaser frame C to the inertial frame I. Note that chaser and target angular velocities $\left({}^I\boldsymbol{\omega}^C\right)_I$ and $\left({}^I\boldsymbol{\omega}^T\right)_I$ are expressed in the inertial frame, while $\left({}^I\boldsymbol{\omega}^C\right)_C = {}^I\boldsymbol{\omega}^C$ and $\left({}^I\boldsymbol{\omega}^T\right)_T = {}^I\boldsymbol{\omega}^T$ are expressed in the respective body-fixed frames. Consequently, the relative angular velocity in C is simply:

$$\delta\boldsymbol{\omega}_C = {}^I\boldsymbol{\omega}^C - \mathbf{R}\,{}^I\boldsymbol{\omega}^T. \tag{11}$$

Finally, it is possible to express the relative attitude dynamics of the chaser with respect to the target, in the chaser body-fixed frame, C, as:

$$\begin{aligned} \delta\dot{\boldsymbol{\omega}}_C = \mathbb{I}_C^{-1}\Big\{ & -[\delta\boldsymbol{\omega}_C\times]\,\mathbb{I}_C\delta\boldsymbol{\omega}_C - [\delta\boldsymbol{\omega}_C\times]\,\mathbb{I}_C\mathbf{R}\,{}^I\boldsymbol{\omega}^T \\ & + \mathbb{I}_C[\delta\boldsymbol{\omega}_C\times]\mathbf{R}\,{}^I\boldsymbol{\omega}^T - [\mathbf{R}\,{}^I\boldsymbol{\omega}^T\times]\,\mathbb{I}_C\delta\boldsymbol{\omega}_C + \mathbf{n}_C \\ & - \mathbf{R}\Big[(\mathbf{R}^{\mathrm{T}}\,\mathbb{I}_C\mathbf{R} - \mathbb{I}_T)\,\mathbb{I}_T^{-1}\,(\mathbf{n}_T - [{}^I\boldsymbol{\omega}^T\times]\,\mathbb{I}_T\,{}^I\boldsymbol{\omega}^T) \\ & + [{}^I\boldsymbol{\omega}^T\times](\mathbf{R}^{\mathrm{T}}\mathbb{I}_C\mathbf{R} - \mathbb{I}_T){}^I\boldsymbol{\omega}^T\Big] - \mathbf{R}\,\mathbf{n}_T\Big\}, \end{aligned} \tag{12}$$

where $\mathbb{I}_C$ and $\mathbb{I}_T$ are the inertia tensors of chaser and target in principal axes; $\mathbf{n}_C$ and $\mathbf{n}_T$ are the external torque vectors acting on the rigid bodies, respectively expressed in C and T [25, 24]. The derivation of the relative attitude kinematics is immediate and analogous to the one for absolute quaternions in Equation (4).

Relative dynamics in Cislunar space can be conveniently expressed in a Local Vertical Local Horizontal (LVLH) reference frame centered on the target along its nominal orbit. The axes of this reference frame are conveniently denoted also as V-bar, H-bar and R-bar, in addition to the usual x, y and z nomenclature. The origin of the LVLH frame is located at the center of mass of the target, and oriented as follows:

- the $z-$axis – named R-bar – is directed from the center of mass of the target towards the center of mass of the Moon;
- the $y-$axis - named H-bar - is in the direction obtained by cross multiplying the R-bar direction with the target's velocity vector, both computed in the Moon centered inertial reference frame. The cross product output corresponds, in analogy with Keplerian orbits, to the specific orbital angular momentum direction, with opposite sign, although such quantity is not directly meaningful for non-Keplerian multi-body orbits;
- the $x-$axis – named V-bar – completes the right-handed triad, and belongs to the plane defined by the target velocity and the radial direction of the target.

The definition of this reference frame comes from a previous literature work [18], with the difference that the radial direction is now towards the Moon and not in the direction of the Lagrangian point of the orbit.

2.2.1. Linearized Relative Dynamics

Linear formulation of the relative dynamics is handy, since guidance, navigation and control functions can be developed exploiting linear techniques and, in general, on-board implementation may exploit linear equations of motion in specific sections of the software (e.g. navigation filters). Therefore, to set up the framework for linear applications, a linearization of the relative dynamics about the target (i.e. reference) spacecraft state can be performed.

Translational relative dynamics can be linearized assuming the relative distance between chaser and target to be small compared to the distance between the target and the primaries: $\|\mathbf{x}\| \ll r_{T_E}$ and $\|\mathbf{x}\| \ll r_{T_M}$ [26]. This condition is likely to be satisfied at all times during typical rendezvous operations, when the relative distance, $\|\mathbf{x}\|$, is below $10^2 - 10^3$ km [27].

The first order expansion of Equation (6) is expressed as:

$$\begin{bmatrix} \dot{\mathbf{x}} \\ \ddot{\mathbf{x}} \end{bmatrix} \approx \begin{bmatrix} \mathbf{0} & \mathbf{I}_{3\times3} \\ \mathbf{\Xi}(t) & \mathbf{0} \end{bmatrix} \begin{bmatrix} \mathbf{x} \\ \dot{\mathbf{x}} \end{bmatrix} + \begin{bmatrix} \mathbf{0} \\ \mathbf{I}_{3\times3} \end{bmatrix} (\delta\mathbf{a}_{4th} + \delta\mathbf{a}_{SRP}) \,, \tag{13}$$

where $\delta\mathbf{a}_{4th}$ and $\delta\mathbf{a}_{SRP}$ are the differential perturbing accelerations, and $\boldsymbol{\Xi}(t)$ is a term dependent on the position of the target spacecraft as:

$$\begin{aligned}\boldsymbol{\Xi}(t) = &-\left(\frac{\mu_E}{r_{T_E}^3} + \frac{\mu_M}{r_{T_M}^3}\right)\mathbf{I}_{3\times3} + 3\frac{\mu_E}{r_{T_E}^3}\left[\hat{r}_{T_E}\hat{r}_{T_E}^{\mathrm{T}}\right] \\ &+ 3\frac{\mu_M}{r_{T_M}^3}\left[\hat{r}_{T_M}\hat{r}_{T_M}^{\mathrm{T}}\right].\end{aligned} \tag{14}$$

Equation (14) is generic and can be used to work with full ephemeris models or with simplified circular or elliptical models, since the differences stay only in the definition of the position vectors of the primaries: as numerical ephemerides or as sinusoidal functions.

Relative attitude Cislunar dynamics can be linearized as in [28]. However, the assumptions to have small attitude errors (i.e. $\delta\mathbf{q} \approxeq [\varepsilon_1, \varepsilon_2, \varepsilon_3, 1-\varepsilon_4^2/2]^{\mathrm{T}}$, where $\varepsilon_1, \varepsilon_2, \varepsilon_3, \varepsilon_4 \to 0$) and small angular rates (i.e. ${}^{I}\boldsymbol{\omega}^{C} \approxeq \mathbf{0}$ and ${}^{I}\boldsymbol{\omega}^{T} \approxeq \mathbf{0}$) are too restrictive for the purposes of this research work. Thus, linearized relative attitude dynamics will not be used in this paper.

2.3. Periodic Orbit Eigen-Spectrum

The complete understanding of the natural dynamical environment in Cislunar space is helpful to support the GNC implementation and to drive the mission design towards better strategies and favorable locations to stage rendezvous operations and proximity trajectories. In these regards, the eigen-spectrum of a periodic orbit, in the Circular Restricted 3-Body Problem (CR3BP) model, is a fundamental feature for trajectory and GNC design. In fact, despite the simplicity of this model, it is capable to provide a significant dynamical insight to analyze the environment characterizing these orbits. Moreover, although the space of eigenvectors and eigenvalues is studied in the CR3BP, the validity of the results may be extended to any more complex model, where deviations from the CR3BP may be seen as perturbations.

Recently, several studies [24, 27, 29] suggested the use of stable, unstable, and center manifolds to perform rendezvous maneuvers. The manifolds computed in the CR3BP can be translated into initial guesses for numerical correction algorithm, and employed to design the corresponding trajectories in the full ephemeris model. Several methods are available for such numerical correction. This research work exploits both single- and multiple-shooting methods [28, 30]: the former are suitable for short, quasi-linear trajectories (e.g. transfer arcs), which can be easily corrected with some iterations of a Newton-Raphson method; the latter are best suited for long-term trajectories (e.g. full orbits), where the propagation of a single arc would result in an excessive amplification of the dynamical non-linearities.

A thorough discussion of CR3BP manifolds is outside the scope of the current paper, and may be found in appropriate literature [31]; for the study at hand, two main phase-space directions will be used [27]:

- the unstable direction, corresponding to an exponential motion away from the reference orbit;
- the center direction, corresponding to a motion along the same orbit.

The set of eigenvectors is completed by the stable direction, not employed in this study. In fact, as passive safety is a key feature of the considered rendezvous problem the stable manifold does not allow for this. A vehicle on the stable manifold will asymptotically approach the target, leading eventually to a collision in case of engine malfunction or misfiring.

It is noted that the aforementioned directions are obtained from 6-dimensional eigenvectors. In a real-world application, the only controlled quantity is the velocity, and it is unrealistic to assume instantaneous position shift within the distance ranges considered in this study. This means that a given position must be reached in the physical space, with a given velocity, such that the 6-dimensional state matches the one dictated by the eigenvector.

Figure 2 depicts the unstable eigenvectors of a sample southern NRHO, splitting the position (i.e. red arrows in Figure 2) and velocity (i.e. magenta arrows in Figure 2) components. This visual representation allows one to understand the different dynamical regimes along the orbit:

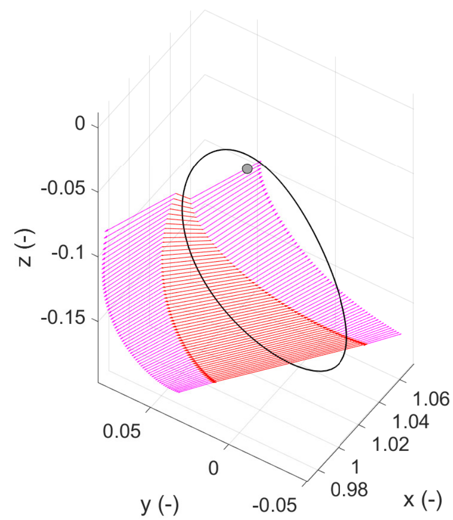

Figure 2: Position and velocity components of unstable eigenvectors along a L2 southern NRHO. Position components with red arrows, originating from the orbital trajectory, velocity components with magenta arrows.

- at the aposelene, the dynamics are slow, and the unstable mode mainly affects the position component;
- moving towards the periselene, the unstable eigenvector becomes more and more significant in the velocity component, as the dynamics scales are faster.

This behavior allows identifying the aposelene as the most suitable region for safe rendezvous, as the slow dynamics is favorable for safe and gradual approach strategies [24, 32, 33, 34].

2.4. Dynamical Models Comparison

Classic 3-body models provide a useful support to perform preliminary analyses, as discussed in Section 2.3; the present discussion aims at proving that they shall be discarded whenever high-fidelity modeling is sought and the goal of the investigation is a practical application on GNC design.

Circular Restricted 3-Body Problem and Elliptic Restricted 3-Body Problem (ER3BP) lack in representing the true motion of the Earth and the Moon, and do not consider the presence of the Sun. These assumptions introduce large errors in the model of the Cislunar dynamics, indeed the real motion of the two primaries results in a variable Earth-Moon eccentricity that is not negligible in dictating the force field that maintains the periodicity of Cislunar orbits. The gravity of the Sun plays a non-negligible role as well; the periodic oscillations of the non-Keplerian orbits due to the Sun's gravitational pull are completely missed out in a 3-body model [35]. The influence of the SRP would have a lower effect on the dynamical results, but it cannot be neglected either for practical applications [36]. On the contrary, the contribution of the irregular lunar gravity field is not considered in this research work, as it is only relevant for low altitude orbits (i.e. less than 750 km) [37]. The presence of the Sun, accounted as a radiation pressure source and as a third-body perturbation on the Earth-Moon barycenter, together with the ephemerides used to obtain the position of the celestial bodies, sets the present discussion in the framework of a Full Ephemeris Restricted 4-Body Problem (FER4BP).

Taking as example the NRHO case, significant deviations between classic 3-body models and FER4BP trajectories are evident. An oscillation of $\sim 5-10$ deg on the "line of orbit apses" is missed whenever the Sun's gravity is not accounted for in the dynamical model [35]. Thus, 3-body models determine an absolute error of ~ 6000 km on the aposelene position, compared with real-world NRHOs. Analogously, circular models, with a constant Earth-Moon eccentricity, generate an absolute error of about 11 000 km km on the NRHO aposelene coordinate [27].

Classic 3-body models are even less rigorous when applied to relative dynamics analysis, compared to FER4BP. The available relative trajectories result to be diverging in the short time, just after few minutes. At large distance from the Moon (e.g. $\sim 10^4$ km), CR3BP and ER3BP trajectories fully diverge from the Full Ephemeris dynamics propagation; underlining how relative dynamics based on simplified dynamical models is misleading with respect to a realistic scenario. The errors are in the order of 500 m, after 1 h of propagation, as can

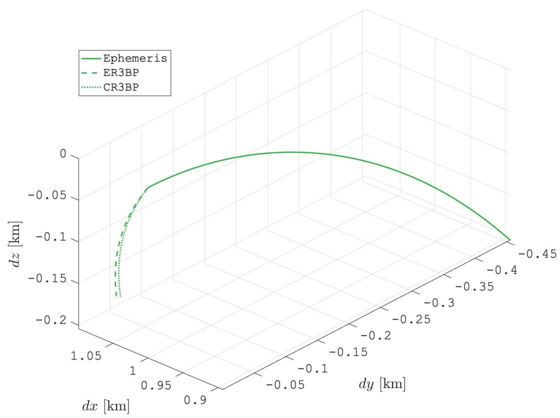

(a) Large distance from the Moon, $\sim 10^4$ km (i.e. NRHO aposelene). Target location out of figure axes.

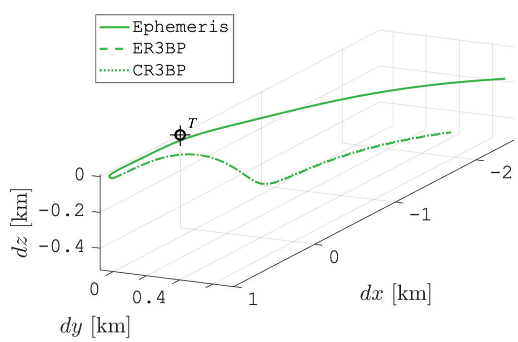

(b) Close distance from the Moon, $\sim 10^3$ km (i.e. NRHO periselene). Target location indicated with label T.

Figure 3: Relative dynamics in Cislunar space propagated for 1 h with CR3BP, ER3BP and FER4BP (Ephemeris) dynamical models to compare the predicted trajectories. The target is orbiting on a L2 NRHO. The initial relative state, $\mathbf{x}$, is 1 km along the $\hat{\mathbf{x}}$ direction of the Synodic reference frame. The target is located at the origin of the relative coordinate frame.

be seen from Figure 3a. In the presented example, the relative motion is initialized with a relative state of 1 km along the $\hat{\mathbf{x}}$ direction of the Synodic reference frame, and the relative dynamics is set in the vicinity of the aposelene of a L2 NRHO. Figure 3b shows an analogous simulation at a closer distance from the Moon (e.g. $\sim 10^3$ km), which is associated with the periselene of a L2 NRHO. In this case, the classic 3-body models have a slower divergence with respect to the FER4BP. However, the error in the relative trajectories is in the order of ~ 100 m after 1 hour of propagation. In general, CR3BP and ER3BP provide worse results in the region of the aposelene of non-Keplerian Earth-Moon orbits, since, at a larger distance from the Moon, the perturbing forces have a stronger effect.

The weak points of the classic restricted 3-body models may be summarized as follows:

- null or constant eccentricity, which has an effect on the aposelene location [27, 38];
- lack the Sun's gravity, which has an effect on the inclination of the "line of orbit apses" [35].

3. Guidance and Control Functions for 6DOF Rendezvous

Guidance and control functions proposed in this paper are based on the direct implementation of the dynamics equations into the guidance and control algorithms. This work is not considering the control actuation and, hence, the discussion about 6DOF guidance and control is concluded when the nominal control acceleration profiles are available. In fact, the output of the control functions is a vector of translational accelerations in inertial frame I and a vector of angular accelerations in chaser body-fixed frame C. These control acceleration vectors, respectively $\mathbf{a}_C$ and $\boldsymbol{\alpha}_C$, are directly summed to the chaser orbit-attitude dynamics. As a consequence, considering the formulation in Equations (6) and (12) or, in alternative, Equation (13) if linearized translational dynamics is used, the controlled relative orbit-attitude dynamics equation are:

$$\ddot{\tilde{\mathbf{x}}} = \ddot{\mathbf{x}} + \mathbf{a}_C, \tag{15}$$

$$\delta\dot{\tilde{\boldsymbol{\omega}}}_C = \delta\dot{\boldsymbol{\omega}}_C + \boldsymbol{\alpha}_C. \tag{16}$$

It shall be noted that the full ephemeris equations are set in an inertial reference frame and the only external quantities are the positions of the celestial bodies; these can be retrieved from Chebyshev series or pre-saved lookup table versions of the ephemerides in order to have a light and fast implementation [39].

3.1. Energy Optimal Guidance and Control

The energy optimal rendezvous problem can be solved because the absolute dynamics of the chaser is controlled by a control variable,

$$\mathbf{u} = \left[\frac{a_{C_x}}{a_{C_x max}}, \frac{a_{C_y}}{a_{C_y max}}, \frac{a_{C_z}}{a_{C_z max}}, \frac{\alpha_{C_1}}{\alpha_{C_1 max}}, \frac{\alpha_{C_2}}{\alpha_{C_2 max}}, \frac{\alpha_{C_3}}{\alpha_{C_3 max}}\right]^{\mathrm{T}}, \tag{17}$$

which is representative of the 6DOF normalized control accelerations, respectively defined in the inertial frame I and in the chaser body-fixed frame C, as the relative controlled equations of motion in Equations (15) and (16). Both are expressed in cartesian coordinates. For sake of simplicity, it is assumed that $a_{C_i max} = 1\,\mathrm{ms}^{-2}$ and $\alpha_{C_j max} = 1\,\mathrm{rads}^{-2}$, for $i = x, y, z$ and $j = 1, 2, 3$. All six controls are bounded: $-\mathbf{1} \leq \mathbf{u} \leq \mathbf{1}$.

3.1.1. Solution of the Optimal Control Problem

Classic solutions of the optimal control problem are based on indirect methods relying on analytical relations and the conditions for optimality require the solution of a two-point boundary value problem. It is well known that indirect methods ensure rapid convergence of good starting guesses, but most of the difficulties are related to the high sensitivity to the initial co-states. The selection of a good initial guess for the co-states is difficult and time consuming, as described in [28].

For the applications discussed in this paper, a more robust method is needed: the optimal rendezvous problem is solved with direct methods, parametrizing only the control variable and converting the optimal control problem into a non-linear programming problem, with a direct transcription process. Direct methods require often a large computation effort, but they are usually robust and can accommodate path constraints.

The solution of a generic non-linear programming problem is a vector of n variables, $\mathbf{p}$, that minimizes a scalar objective function:

$$\min_{\mathbf{p}} F(\mathbf{p}), \tag{18}$$

subject to m equality or inequality constraints:

$$\mathbf{b}_l \leq \mathbf{c}(\mathbf{p}) \leq \mathbf{b}_u, \tag{19}$$

and bounds:

$$\mathbf{p}_l \leq \mathbf{p} \leq \mathbf{p}_u. \tag{20}$$

The equality constraints are obtained imposing $\mathbf{b}_l = \mathbf{b}_u$.

With direct methods, the differential dynamic constraints of the indirect optimal rendezvous problem are converted into a set of algebraic constraints.

3.1.2. Numerical Implementation

The optimality in terms of minimum energy control (i.e. minimum quadratic) is achieved defining the scalar objective function in Equation (18) as:

$$F(\bar{\mathbf{p}}) = \frac{1}{2} \int_{\bar{t}} \mathbf{u}|_{\bar{\mathbf{p}}}^{\mathrm{T}}(t)\; \mathbf{u}|_{\bar{\mathbf{p}}}(t)\, dt, \tag{21}$$

where $\bar{t}$ is the rendezvous time from t_0 to t_f. The integral is computed numerically, from the control parametrization functions, knowing just the value of $\bar{\mathbf{p}}$.

A constrained minimization algorithm is applied to solve the non-linear programming problem associated with the direct transcription of the optimal control. The algorithm exploits a sequential quadratic programming (SQP) method to solve the rendezvous. The initial guess for the parameters in the vector $\mathbf{p}$ is random, normally distributed within the bounds for the parameters. The initial guess for the rendezvous time of flight (TOF) is given according to the desired order of magnitude for t_f. The differential equations are integrated with a variable-step, variable-order (VSVO) Adams-Bashforth-Moulton solver.

3.1.3. Control Parametrization

The rendezvous path can be discretized in multiple arcs connected by patch points and, without increasing the complexity of the control actions, different parameterizations are possible. In this research work, best results have been obtained with polynomials and Fourier series representations. Polynomials up to the third degree and Fourier series up to the fourth order are proposed. The limitations in the degree of the expansions are motivated to limit the number of involved parameters, thus, the dimension n of the non-linear programming (NLP) problem. The control parametrization with a second-degree polynomial for the translational control and a with a fourth order Fourier series for the rotation control results in:

$$\mathbf{a}_C(t) = \mathbf{a}_0 + \mathbf{a}_1 \left(\frac{t}{t_{ref}}\right) + \mathbf{a}_2 \left(\frac{t}{t_{ref}}\right)^2, \tag{22}$$

$$\boldsymbol{\alpha}_C(t) = \frac{\boldsymbol{\alpha}_0}{2} + \sum_{k=1}^{4} \left[\boldsymbol{\alpha}_k \cos\left(k\boldsymbol{\tau}\frac{t}{t_{ref}}\right) + \boldsymbol{\beta}_k \sin\left(k\boldsymbol{\tau}\frac{t}{t_{ref}}\right)\right], \tag{23}$$

where $\mathbf{a}_l$ for $l = 0, 1, 2$, $\boldsymbol{\alpha}_m$ for $m = 0, 1, 2, 3, 4$, $\boldsymbol{\beta}_n$ for $n = 1, 2, 3, 4$, and $\boldsymbol{\tau}$ are 3×1 parameters vectors defined, respectively, in the reference frames I and C. The reference time, t_{ref}, is needed to non-dimensionalize the time, t, in the parametrized control functions. The physical dimensions of these parameters are defined according to the physical quantity they are parametrizing. These parameters compose the vector of unknown variables, $\mathbf{p} = \left[\mathbf{a}_l^{\mathrm{T}}, \boldsymbol{\alpha}_m^{\mathrm{T}}, \boldsymbol{\beta}_n^{\mathrm{T}}, \boldsymbol{\tau}^{\mathrm{T}}, t_f\right]^{\mathrm{T}}$, to be found solving the problem in Equation (18). The choice of a reference time equal to the rendezvous arc time of flight, $t_{ref} = t_f$, has proved to work effectively [28]. In this case, the dimension n of the NLP associated to the energy optimal rendezvous problem is 40: 9 are the parameters for $\mathbf{a}_C(t)$, 30 are the parameters for $\boldsymbol{\alpha}_C(t)$ and 1 parameter is t_f.

Alternative control parameterizations have been investigated in previous literature works [24, 28, 40], but the one discussed in this section guarantees a good compromise between robustness and fast convergence of the guidance and control algorithm for the considered example applications. The authors suggest leaving enough freedom in setting the control parametrization for alternative problems. However, in general, the one presented in this paper shall be considered as an upper level for the parametrization complexity, since more elaborated control laws typically converge to simpler ones, providing computed solutions with negligible higher degree terms in the series. The usage of shorter expansion shall be carefully supervised to exclude the risk of sub-optimal over constrained solutions, in particular when non-linear perturbed dynamics is used.

3.1.4. Rendezvous Constraints

The constraints in Equation (19) are obtained from numerical integration of the controlled rendezvous dynamics in Equations (15) and (16). In fact, given a generic vector $\bar{\mathbf{p}}$ the relative dynamics has a certain evolution; the relative states at the end of the particular rendezvous simulations have to satisfy the imposed boundary conditions at the final time. The non-linear FER4BP controlled dynamics is used for rendezvous constraints evaluation.

In practical rendezvous scenarios, the position vector of the docking/berthing point will be likely displaced from the center of mass of the target spacecraft. It follows, the docking boundary condition at final time will be related to the 6DOF configuration of the lunar gateway driven by its absolute orbit-attitude dynamics. The definition of an error state vector, $[\mathbf{x}_\epsilon; \dot{\mathbf{x}}_\epsilon; \delta\mathbf{q}_\epsilon; \delta\boldsymbol{\omega}_\epsilon]$, between the relative orbit-attitude state of the chaser and a desired final relative condition, $[\mathbf{x}_d; \dot{\mathbf{x}}_d; \delta\mathbf{q}_d; \delta\boldsymbol{\omega}_d]$, allows applying the boundary conditions to any rendezvous problem:

$$\begin{cases} \mathbf{x}_\epsilon & = \mathbf{x}(t_f) - \mathbf{x}_d \\ \dot{\mathbf{x}}_\epsilon & = \dot{\mathbf{x}}(t_f) - \dot{\mathbf{x}}_d \\ \delta\mathbf{q}_\epsilon & = \delta\mathbf{q}(t_f) \times \delta\mathbf{q}_d^{-1} \\ \delta\boldsymbol{\omega}_\epsilon & = \delta\boldsymbol{\omega}(t_f) - \delta\boldsymbol{\omega}_d. \end{cases} \tag{24}$$

In particular, all the relative states in Equation (24) can be obtained directly with a difference from the desired final condition, except for the quaternions which require the successive rotation operator. Then, the null final condition can be applied to the error state vector. During the study, faster convergence properties have been observed when the constraint on the final relative quaternion is not enforced in vectorial form as $\delta\mathbf{q}(t_f) = [\mathbf{0}, \pm 1]$, or $\delta\mathbf{q}_\epsilon = [\mathbf{0}, \pm 1]$, but in scalar form: $H(\delta q_4(t_f)) = 1 - \delta q_4^2(t_f) = 0$, or $H(\delta q_{\epsilon_4}) = 1 - \delta q_{\epsilon_4}^2 = 0$, where $H(\cdot)$ is the scalar quaternion constraint function.

4. Vision-based Navigation Functions for 6DOF Rendezvous

Navigation functions, similarly to what has been discussed for the guidance and control functions in Section 3, are based on 6DOF equations of motion in multi-body gravitational environment. A vision-based only navigation technique is presented in this paper to prove its feasibility for applications in Cislunar environment. This is motivated by the fact that it can be integrated with the 6DOF guidance and control functions, by exploiting a single navigation architecture based on optical sensors, to estimate both translational and rotational relative states. Moreover, it guarantees the largest applicability of the proposed methods, with passively cooperative spacecraft, or even with non-cooperative or unknown targets. The only constraint of vision-based navigation is related with the relative distances between the two spacecraft. Thus, despite the broad range of distances involved during terminal rendezvous operations in Cislunar orbits, the navigation techniques introduced in this section are suitable for short distances relative navigation approaches (i.e. $< 1\,\mathrm{km}$). At far-range, coupled 6DOF navigation is typically not considered and the relative states estimation is based on alternative navigation techniques [41].

4.1. Vision-based Navigation Architecture

The navigation algorithm assumes that the only available data are provided by two cameras placed on the chaser and by markers located on the target, but it can be easily extended to different visual navigation settings. In principle, a

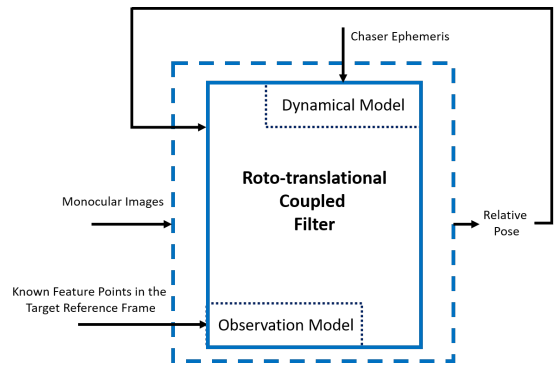

Figure 4: Relative navigation architecture: block diagram.

known pattern of markers can provide closed-form solution of the P-n-P problem. However, the architecture with a stereo camera, allows us to easily adapt the algorithm and extend it to approaches around unknown objects. The chaser is assumed to collect and track N known feature points on the target. The adopted reference frames for both target and chaser are introduced in Section 2.

The proposed architecture for relative navigation of a chaser satellite with respect to a passively cooperative target is summarized in the block diagram in Figure 4.

This architecture is tightly coupled. In fact, the measurements are directly processed by the navigation filter. The filter processes the features extracted by the two cameras to compute the relative target/chaser position and attitude. In the observation model of the camera, the knowledge of feature points on the target is assumed. Since the observation model depends on both position and attitude of the target spacecraft, the navigation filter has to be coupled and non-linear.

4.1.1. Dynamical Model

The state vector of the filter is defined as:

$$\mathbf{v} = [\mathbf{x}^{\mathrm{T}},\ \dot{\mathbf{x}}^{\mathrm{T}},\ \delta\mathbf{q}^{\mathrm{T}},\ \delta\boldsymbol{\omega}_C^{\mathrm{T}}]^{\mathrm{T}}, \tag{25}$$

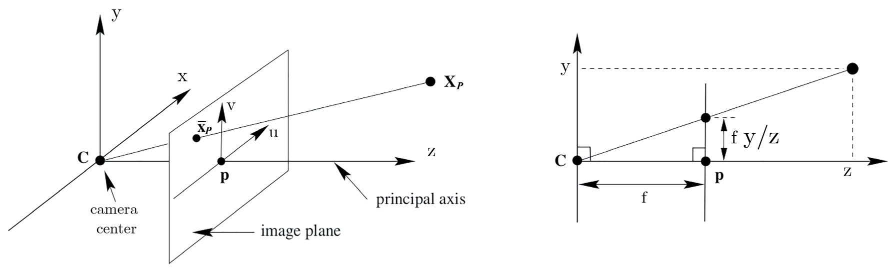

Figure 5: Pinhole camera model.

from the 6DOF relative states defined in Section 2.2. The state dynamics inside the filter is assumed to evolve according to the models presented in Section 2.2.1. In particular, for the relative translational dynamics, the linearized model without perturbations, in Equation (13), is adopted. For the rotational dynamics, the relative attitude in Equation (12) is used, assuming a perturbation-free motion.

4.1.2. Observation Model

A simple pinhole model [42] was used as camera model. It assumes that all the light rays travel through an infinitely small hole and are projected onto an image frame. No lenses are used to focus the light and, therefore, distortion is not considered. Using prospective geometry rules, it is possible to mathematically describe the relationship between the 3D coordinates of a generic point and the 2D coordinates of its projection onto the image plane of the camera.

Looking at Figure 5, a derivation of how the coordinates of the point $\bar{\mathbf{x}}_P = [u, v]$, in the image plane, depend on the coordinates of a real-world point, $\mathbf{X}_P = [x, y, z]$, is provided. Assuming the chaser body-fixed reference frame C aligned with the left camera center of projection, and to have a stereo rig composed by two cameras, with focal length f, separated by a given baseline b, the following expressions are derived:

$$u_L(i) = f\frac{x_i}{z_i} \tag{26}$$

$$v_L(i) = f\frac{y_i}{z_i} \tag{27}$$

where $u_L(i)$ and $v_L(i)$ are the u, v coordinates in the image plane of the left camera, with $\boldsymbol{\rho}_i = [x_i, y_i, z_i]$ being a generic feature point in the chaser frame C. Similarly, for the right camera:

$$u_R(i) = f\frac{x_i + b}{z_i} \tag{28}$$

$$v_R(i) = f\frac{y_i}{z_i} \tag{29}$$

Finally, $\mathbf{l}_{Li} = [u_L(i),\, v_L(i)]$ and $\mathbf{l}_{Ri} = [u_R(i),\, v_R(i)]$ can be defined. Given this camera model, at each time step, the discrete measurement vector provided by the cameras is:

$$\mathbf{z}_i = [\mathbf{l}_{Li},\ \mathbf{l}_{Ri}] \tag{30}$$

Please, keep in mind that $\mathbf{z}_i$ is function of the relative 6DOF state being $\boldsymbol{\rho}_i = {}^C\mathbf{A}^I\,\mathbf{x} + \mathbf{R}(\delta\mathbf{q})\boldsymbol{P}_i$, where $\boldsymbol{P}_i$ is the position vector of the i-th feature point in the target body-fixed frame T.

4.1.3. Estimation Procedure

The assumed observation model is non-linear. For this reason, it is necessary to adopt a non-linear filtering technique. The more common techniques, i.e. Extended Kalman Filter (EKF) and Unscented Kalman Filter (UKF), were taken into account. One of the main drivers for navigation filters is their computational cost. Thus, an EKF, instead of an UKF, has been adopted. In fact, for the latter filter, the state dynamics have to be propagated at each time step for $2n$ sigma points, where n is the number of states ($n = 13$ in this case).

5. Rendezvous Scenario

Operational concepts for rendezvous with a large space structure in Cislunar space have been recently proposed by different authors [29, 18], who highlighted the relevance of orbit-attitude coupling in the rendezvous GNC design. This outcome is also applicable to Earth orbits rendezvous with extended space infrastructures [43, 44].

A rendezvous application scenario with a passively cooperative target orbiting on a lunar L2 NRHO, with an orbital period of $\sim 7\,\mathrm{d}$ and periselene altitude of $\sim 3000\,\mathrm{km}$, is discussed in this research work, in accordance with existing feasibility studies about the Lunar Gateway. The case study is used to present the GNC developments proposed in this paper, to define an ideal rendezvous strategy, and to quantify a possible set of rendezvous trajectories that are inherently safe and optimized in terms of required ΔV.

Specifically, the terminal rendezvous operations can be macroscopically divided into three phases identified by the order-of-magnitude of the relative distances between chaser and target:

1. Far-range rendezvous, from $\sim 10\,000\,\mathrm{km}$ to a $100\,\mathrm{km}$ distance;
2. Close-range rendezvous, from $100\,\mathrm{km}$ to $1\,\mathrm{km}$ distance;
3. Final approach rendezvous, from $1\,\mathrm{km}$ up to docking/berthing with the target.

During far-range rendezvous the chaser is controlled in absolute position, with open-loop impulsive maneuvers for orbit control, while the relative GNC starts to be effective from the close-range phase. The goal of the far-range rendezvous is to reach a final state relative to the target spacecraft, defined according to its motion on the operational orbit. Hence, the far-range rendezvous is also exploited to accurately phase the two spacecraft before the close-range rendezvous. In this phase, the chaser attitude state is completely decoupled from the one of the target, and it is defined to satisfy the chaser system requirements.

Close-range rendezvous begins with a departure from a holding-point. The position of the chaser is controlled relatively to the one of the target, impulsive and continuous thrust maneuvers are used. Attitude state is still decoupled from the target rotational motion, however, the orientation of the chaser is defined to satisfy optical navigation requirements.

Final approach rendezvous is entirely within the domain of a coupled 6DOF GNC, with optical navigation techniques. The low relative distances between chaser and target requires continuous closed-loop forced translation for safety reasons. Final approach rendezvous is further subdivided in a closing phase to acquire a holding-point which is geometrically in line with the docking/berthing point, and in a final translation keeping the chaser attitude aligned with the one of the target. During the whole final approach rendezvous, the attitude control is entirely coupled with the position control in order to satisfy navigation (e.g. camera pointing) and docking (e.g. docking port alignment) requirements.

5.1. Rendezvous Guidance and Control

Rendezvous trajectories are computed exploiting the dynamics and the GNC functions as described in the previous sections. The different rendezvous phases are associated to different guidance and control functions, as will be discussed hereafter.

5.1.1. Far-range

The chaser (i.e. automated transfer vehicles) will have to reach the target (i.e. Cislunar gateway) from different locations, such as the Earth, the Moon or a different non-Keplerian orbit, within a reasonable time and cost. Therefore, a preliminary analysis involves the design of a trajectory connecting the departure point with the desired rendezvous location. Far-range rendezvous starts, nominally, at a holding point HP_0, located 10 000 km away from the target vehicle. A dedicated phasing according to the departure point of the chaser shall be designed in order to synchronize the chaser spacecraft on the operational orbit of the target at the holding point HP_1, reaching a relative distance of about 100 km. A description of feasible phasing strategies was treated by Bucci [32].

The rationale behind the present study is the passive safety of the considered trajectories, i.e. guaranteeing that the natural motion of the chaser vehicle does not approach the target in case of missed maneuver. Thus, the center eigenvector is deemed the most suitable direction to locate both HP_0 and HP_1

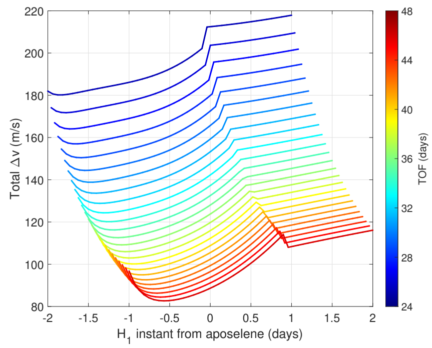

Figure 6: Parametric analysis of ΔV needed to connect HP_0 and HP_1.

point: targeting this phase-space direction, a vehicle will hover around the target in a safe way, neither approaching nor going away from it. This dynamical behavior allows for safe go/no-go windows, hovering motion, inspection, and other activities or contingencies that need time while in proximity of the target. Furthermore, the center eigenvector denotes infinite locations on the center manifold of the orbit. The holding point may be placed according to a given criterion; within this study, such criterion is the distance from the target at the beginning of the arc.

The location of HP_0 and HP_1, together with the TOF employed to connect the two points, dictate the total ΔV budget needed for such arc. Figure 6 depicts a parametric plot:

- The horizontal axis represents the location of HP_1. Using the aposelene as reference point for the rendezvous sequence, the location of HP_1 is given in days before the aposelene.
- The color code parametrizes the time of flight between HP_0 and HP_1.
- The vertical axis report the corresponding ΔV for such connection.

The ΔV depends, naturally, also on the distances of HP_0 and HP_1 from the target. The presented parametric study does not consider variations of that distance, which nevertheless have a minor impact on the ΔV budget.

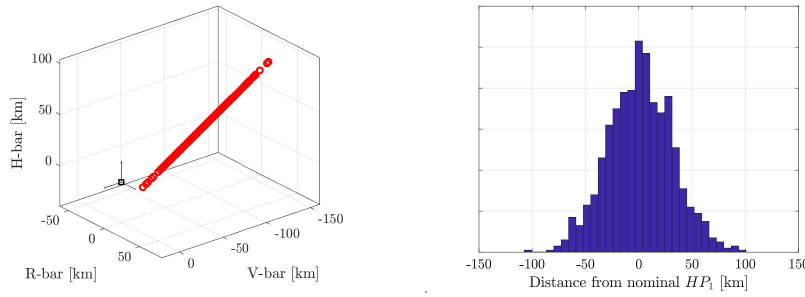

(a) Dispersion of HP_1 location.

(b) Signed distance from nominal HP_1 location.

Figure 7: Monte Carlo analysis of far-range rendezvous.

Furthermore, it is noted that the maneuver at HP_0 will, generally, be affected by an execution error. The transfer will then need correction, since HP_1 will be reached before or after the nominal time, with a given dispersion. Figure 7a depicts a Monte-Carlo analysis, showing the cloud of points reached by an open-loop far-range transfer, implementing an hypothetical 0.5% magnitude error on the maneuver at HP_0.

The dispersion can be mitigated, by tuning the actual location of HP_1 to take into account the 3σ variation of its position, or, conversely, by tuning the time of flight. As noted by the aligned pattern depicted in Figure 7a, all the points are clustered along the relative velocity direction. Additionally, Figure 7b depicts the histogram of the distance reached after the nominal time of flight, which can be correlated to time error as the relative velocity is known. The sign of the distance indicates the location prior or after the nominal point. A precise targeting of HP_1 would require correction maneuvers in order to begin the close-range rendezvous phase as close as possible to the nominal holding location. This is intrinsically related to the open-loop impulsive rendezvous maneuvers characterizing the far-range phase.

5.1.2. Close-range

The nominal start of the close-range phase is denoted by the holding point HP_1, 100 km away from the target. The close-range rendezvous is performed with two impulsive maneuvers to connect the holding point HP_1 to the holding point HP_2, at 1 km from target. The current strategy is motivated by a minimization of the rendezvous ΔV and by the passive safety enforcement.

Passive safety is guaranteed by designing HP_1 on the center manifold direction, as described previously in Section 5.1.1. The arrival point for the close-range rendezvous, HP_2, lies on the unstable manifold of the target orbit. With this strategy, if failures occur after reaching HP_2 and no departure burn is performed, the chaser will safely start drifting away with a spiralling relative motion from the target without entering the Keep-out-Sphere (KOS) with radius 1 km, as shown in Figure 8. Moreover, if no braking burn occurs, the chaser will safely go away without getting closer to the target. Note that the former condition not only allows one to avoid a dangerous close proximity of the chaser to the target, but it also allows for a subsequent chance to again perform the transfer to HP_2. In fact, the unstable manifold guarantees a safe drift away, but its time scale is slow enough to allow recovery (e.g. 10 km in a NRHO orbital period of 7 d). It is remarked that, if the final approach rendezvous phase is not started immediately after the completion of the close-range rendezvous phase, an active station keeping action must be performed to avoid the departure of the chaser in the unstable manifold direction.

Along the close-range rendezvous trajectory, between HP_1 and HP_2, the chaser may not exactly lie on the unstable manifold direction, approaching from a holding point on the center one. Hence, the passive safety drift could be not guaranteed in any case. Moreover, an error in the direction of the maneuver execution, may lead to dangerous approaching trajectories. In these cases, the passive safety design can be coupled with a closed-loop control that can enforce active safety at any time [27]. However, the unstable modes are predominant over the center ones [31], especially within the assumptions of FER4BP, where

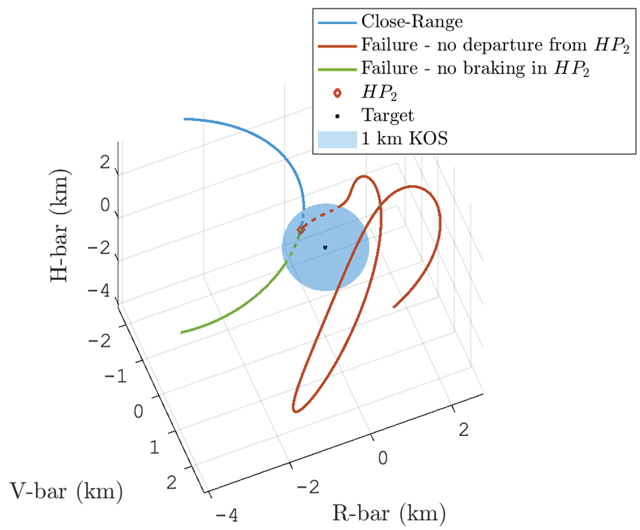

Figure 8: Close-range rendezvous final part: arrival at HP_2 with failures and passive safety enforcement. None of the trajectories enter inside the KOS.

every non-CR3BP acceleration may be considered as a perturbation that triggers the divergent motion away from the target. Furthermore, the long time scales of the natural motion (i.e. in the order of days) always allow ample time window for contingency recoveries. These considerations thus support the passive safety design logic.

Figure 9 shows the close-range rendezvous arc in the relative LVLH frame and highlights the chaser approaching the target from the negative V-bar, with a free drift motion in the 3-dimensional LVLH space. This picture is relevant to understand the relative distance between chaser and target during close-range rendezvous phase. The arc from HP_1 and HP_2 is computed in open-loop, optimizing the 2-burns impulsive maneuvers to perform it. The ballistic arc allows time for orbit determination and navigation, in order to reduce the dispersion on the state at HP_2. The position of this holding-point is set on the 1 km KOS, which is sufficient to guarantee the keep-out condition at 3σ with a navigation dispersion of 100 m and 1 cm/s (3σ).

In alternative, close-range rendezvous can be performed exploiting continu-

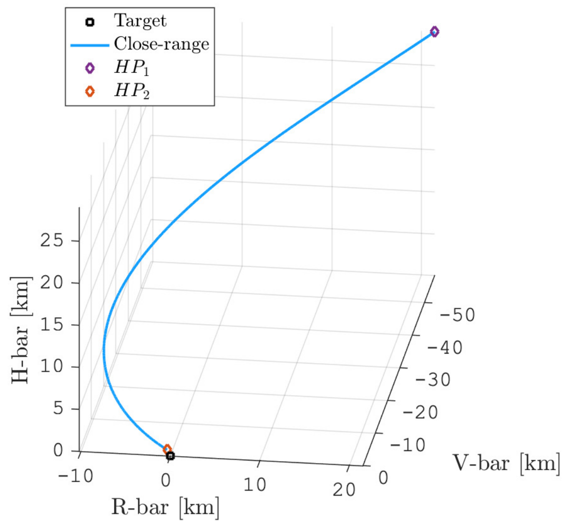

Figure 9: Close-range rendezvous with impulsive maneuvers.

ous thrust maneuvers. The continuous thrust trajectory is designed and optimized with the guidance and control algorithms described in Section 3.1. Despite the fact that these algorithms are developed for the final translation phase of the rendezvous, they can be applied also to close-range phase, when cross-link relative navigation data are present. In this case, the rendezvous trajectories are computed exploiting fully relative guidance and control methods in closed-loop; while, in the impulsive case presented before, the rendezvous trajectories are obtained with an open-loop targeting method on the final relative position state.

Figure 10 shows the close-range trajectory with continuous thrust closed-loop control, which is different from the analogous in Figure 9. The forced motion provides a more direct path to the second holding point, avoiding the $\sim 10\,\mathrm{km}$ overshoot on the negative R-bar direction.

The presented continuous thrust rendezvous in Figure 10 is optimized in terms of ΔV. However, this rendezvous strategy requires higher ΔVs with respect to the impulsive one; it is convenient in terms of time of flight and in terms of control over the rendezvous path, since it does not have any ballistic

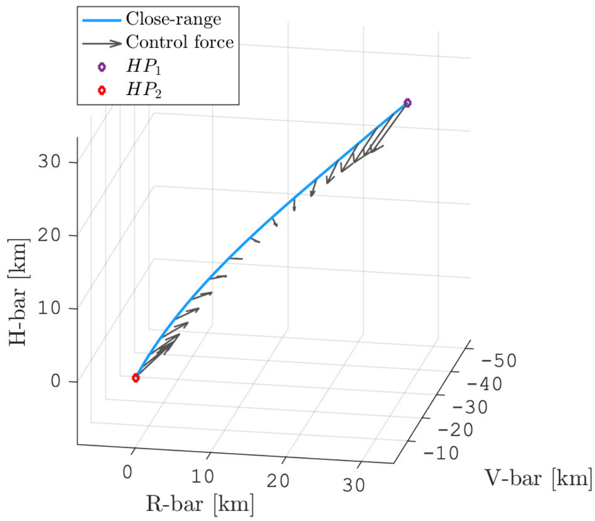

Figure 10: Close-range rendezvous with continuous thrust.

arc driven by the natural dynamics. Moreover, closed-loop continuous thrust rendezvous is more robust with respect to execution errors and the final targeting point is achieved within the accuracy of the GNC subsystem.

The required ΔV and TOF to perform close-range rendezvous is reported in Table 1, both for impulsive strategy and for continuous thrust strategy.

5.1.3. Final Approach

The final approach phase begins at the limit of the KOS and it considers a full relative 6DOF GNC with path constraints. This last phase is characterized by a forced motion actuated by a closed-loop 6DOF control, with vision-based relative navigation.

Table 1: Close-range ΔV and TOF.

	Impulsive	Continuous
ΔV	2.78 m/s	8.74 m/s
TOF	20 h	10 h

The final approach phase is actually subdivided in two sub-phases: the closing sub-phase and the final translation sub-phase. The former connects HP_2 on the 1 km KOS with a point, HP_3 of the Final-Approach-Sphere (FAS), which is a further keep-out-zone separating the final translation.

The FAS is set at 200 m from the target, which is sufficient to guarantee the keep-out condition at 3σ with the navigation dispersion lower than 1 m and 0.1 cm/s (3σ), as discussed in Section 5.2. Inside the FAS, the trajectory is assumed to be a straight line in LVLH reference frame along the docking/berthing point axis. In this paper, a final translation along the R-bar is presented. However, no particular difference exists if the V-bar or the H-bar is selected: the forced motion completely overcome the extremely slow dynamics at the aposelene of NRHO. In addition, inside the FAS the maximum relative velocity allowed by the GNC functions is 10 cm/s, so that a Collision Avoidance Maneuver (CAM) can be performed in time if any failure occurs (e.g. wrong direction/magnitude of the control action). The trajectories of the closing and the final translation sub-phases are reported in Figure 11, while ΔVs and TOFs are listed in Table 2. Figure 12 shows relative distance and relative velocity trends during the final approach phase. The constraints on the maximum relative velocity during the final translation sub-phase are respected.

Inside the KOS, the pointing of the cameras and the alignment of the docking mechanism of chaser are mandatory for a correct rendezvous maneuver. Figure 13 shows relative quaternion and relative angular velocity in the final approach phase. During the closing sub-phase, the attitude of the chaser is aligned and synchronized with the one of the target spacecraft, in preparation

Table 2: Final Approach ΔV and TOF.

	Closing	Final translation
ΔV	0.81 m/s	0.16 m/s
TOF	1 h	1 h

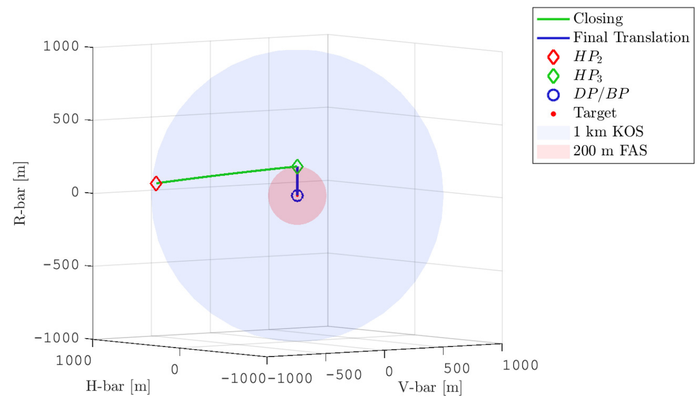

Figure 11: Final approach rendezvous.

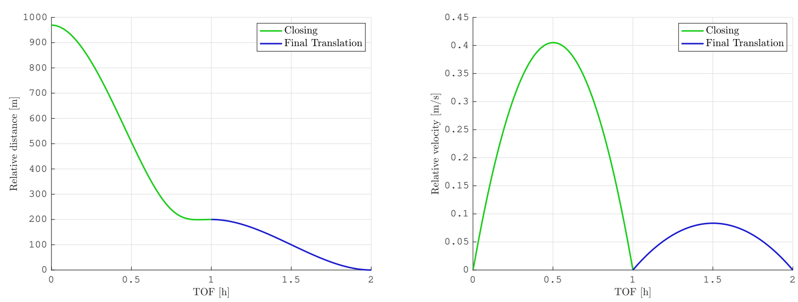

(a) Relative position.

(b) Relative velocity.

Figure 12: Final approach rendezvous: linear motion.

of the final translation, which is characterized by a null relative attitude dynamics.

The nominal absolute attitude of the target is related to its system requirements. At the aposelene of the NRHO, the rotational dynamics is extremely slow, as discussed in [16, 45]. Accurate attitude control actuators are required; angular momentum exchange devices are suggested for the final approach attitude control. In the presented scenario, the angular momentum to exchange is lower than 100 Nms.

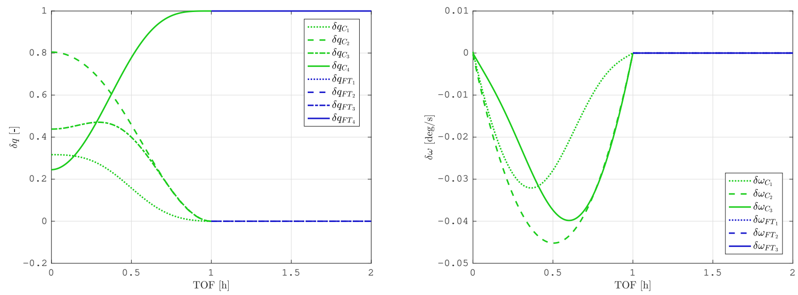

(a) Relative quaternion.

(b) Relative angular velocity.

Figure 13: Final approach rendezvous: rotational motion.

5.2. Rendezvous Navigation

Navigation during rendezvous is dependent from the actual rendezvous phase, according to the relative distance between chaser and target. The proposed vision-based navigation techniques apply to the final approach phase. A discussion on navigation at larger distances, when coupled 6DOF visual navigation is not applicable, is included to have a complete overview of the proposed rendezvous GNC.

5.2.1. Far-range and Close-range

Far-range and close-range rendezvous phases can be associated to operations where the relative distance between chaser and target does not allow optical navigation (i.e. greater than 1 km). In these cases, orbit determination is typically obtained by considering Earth-based measurements.

However, in the last decades, several different methods for autonomous orbit determination have been proposed. These methodologies can be divided into *individual autonomy*, when a single spacecraft can estimate its own state, and *constellation autonomy* when through relative measurements it is possible to obtain the state estimation of the complete constellation simultaneously. From the 80's, the main space agencies were interested in proposing sensors and algorithms to introduce individual autonomy for orbit determination [46]. Most of the proposed techniques for individual autonomy are based on sensing the vector to a large body, such as the direction of the Earth, Earth's limb [47] or Earth's magnetic field [48] and even X-ray pulsars [49]. To guarantee constellation autonomy, useful during close-range phase, it is necessary to add some relative measurements. These additional measurements can include angles to the other spacecraft obtained by optical tracking, cross-link range or doppler. The use of a cross-link in a constellation to enhance navigation was first introduced by Markley [50]. Yim [51], instead proposed autonomous orbit determination using only optical trackers without, however, guaranteeing the same estimation accuracy. One of the most common navigation techniques for non-Keplerian orbits is the liaison method, introduced by Hill & al. [41]. In their study, they present an autonomous relative navigation technique exploiting only cross-link range without any ground tracking. This kind of navigation technique, however, is applicable only to specific relative orbits. Summarizing, for far-range navigation, the proposed baseline is to use ground tracking for the chaser spacecraft, and to include also relative cross-link measurements for relative navigation at close-range.

5.2.2. Final Approach

The final approach phase is considered as simulation scenario for the validation of navigation functions in Section 4. Short distances are needed to resolve the target in the sensor frame with the desired resolution to apply precise image processing techniques. In fact, the vision-based relative navigation can be applied only when the target is sufficiently large on the camera sensor. This condition is dictated by the dimension of the target, the field of view, the resolution and the baseline between the cameras. In this study, a portion of the final approach ranging from 200m to 10m (i.e. the final translation sub-phase) has been considered.

The proposed relative navigation architecture is validated through numerical simulations. The relative translational dynamics between the two spacecraft is reproduced by integrating the full non-linear equations, including perturbations effect. For the relative rotational dynamics, equations introduced in

Section 2.2.1 are used considering, also in this case, the perturbations acting on the spacecraft.

5.2.3. Measurement Generation

In order to evaluate the performance of the proposed navigation filter, simulated sets of 2D point features are generated. Specifically, N 3D feature points are randomly generated on the target according to a uniform distribution along each of the three axes, considering the target dimensions. The evolution of these points in the chaser reference frame $\mathcal{C}_{Cl}$ is then computed according to the true relative position and attitude. Hence, the 3D position of each detected feature point is projected on the image plane of the right and left camera. The obtained 2D coordinates are modified to account for potential errors introduced by the image processing. Also in this case, a Gaussian white noise is added to the pixel coordinates of each point feature, whose standard deviation (σ_{pix}) is expressed in terms of a certain number of pixel. In this work, the focal length is assumed equal to $f = 30mm$ and a camera resolution of 2048 x 2048.

5.2.4. Feature Points

A set of M feature points on the target spacecraft are assumed to be known. These points can be representative of LEDs or visual markers placed on the target spacecraft. This set of points is extracted uniformly at each simulation to test the filter robustness for random configurations of feature points. For the numerical validation, uniform extraction of the feature points has been assumed within the following boundaries: $b_x = [-1.2; 1.2]$, $b_y = [-2; 2]$, $b_z = [-1.2; 1.2]$.

5.2.5. Results

The relative position error is defined as:

$$e_\rho = \sqrt{(x_i - \hat{x}_i)^2 + (y_i - \hat{y}_i)^2 + (z_i - \hat{z}_i)^2} \tag{31}$$

where $\hat{x}, \hat{y}, \hat{z}$ are the position components estimates.

And the relative attitude error is computed as:

$$e_\theta = 2\cos^{-1}(q_{e_0}) \tag{32}$$

where in our notation, q_{e_0} is the scalar part of the error quaternion $\mathbf{q}_e = \mathbf{q} \times \hat{\mathbf{q}}^{-1}$.

5.2.6. Nominal Scenario

For the nominal scenario, a statistical analysis of 50 runs has been conducted. The initial conditions are extracted from a Gaussian distribution with mean equal to the true state and covariance given by the initial state covariance matrix $\mathbf{P}$. The initial state covariance matrix $\mathbf{P}$ is selected as:

$$\mathbf{P} = diag([{\sigma_\rho}^2, {\sigma_{\dot{\rho}}}^2, {\sigma_q}^2, {\sigma_\omega}^2]) \tag{33}$$

with:

- ${\sigma_\rho}^2 = [1,\ 1,\ 1]\ m$
- ${\sigma_{\dot{\rho}}}^2 = [1,\ 1,\ 1] \cdot 10^{-1}\ m/s$
- ${\sigma_q}^2 = [1,\ 1,\ 1,\ 1] \cdot 10^{-5}$
- ${\sigma_\omega}^2 = [1,\ 1,\ 1] \cdot 10^{-1}\ deg/s$

The filter is run at 1Hz with a noise associated to the feature extraction of $\sigma_{pix} = 1$. In this first simulation, a set of 25 feature points is considered. Figures 14a and 14b show mean relative position and attitude errors, averaged for each time step over the 50 runs.

Figures 14a and 14b show a fast convergence of the filter and acceptable errors if considering close approach or monitoring scenarios. In particular, the error in the estimation of the relative position is lower than $0.1m$ and the relative attitude error is always lower than $0.2°$ at steady state.

5.2.7. Noise Sensitivity Analysis

The robustness of the proposed algorithm over the noise value is analyzed. A sensitivity analysis over σ_{pix} is performed. The nominal scenario is propagated with a noise standard deviation ranging from 0.5 to 2.5 pixels. This value is the measurement noise associated and added to each of the feature points during

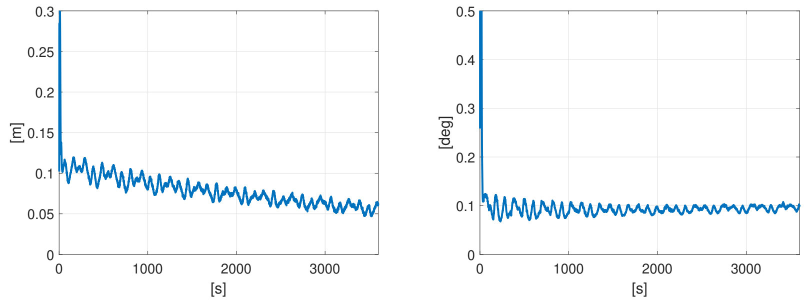

(a) Average relative position error. (b) Average relative attitude error.

Figure 14: Navigation errors: final translation sub-phase from 200 m to 10 m.

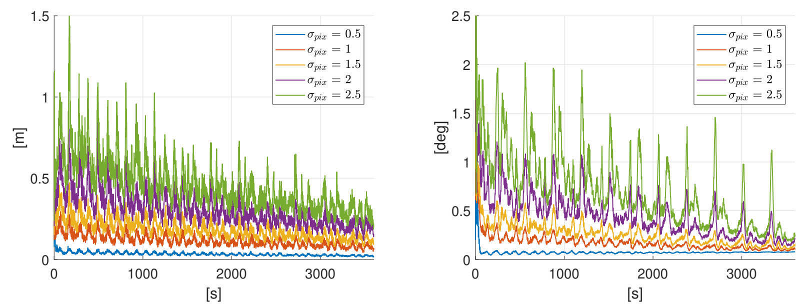

(a) Average relative position error. (b) Average relative attitude error.

Figure 15: Noise sensitivity analysis.

the measurements generation. The initial conditions and the tuning of the filter are kept constant for all the different test cases. The results of such analysis are shown in Figures 15a and 15b, where the errors associated with the feature extraction noise of the nominal scenario (i.e. $\sigma_{pix} = 1$) are almost identical to those reported in Figures 14a and 14b, even if the scales of the vertical axes in the plots are different.

As expected, both relative position and attitude errors increase with increasing noise level. Also in the most pessimistic considered case, the filter is able to correctly estimate the relative spacecraft pose.

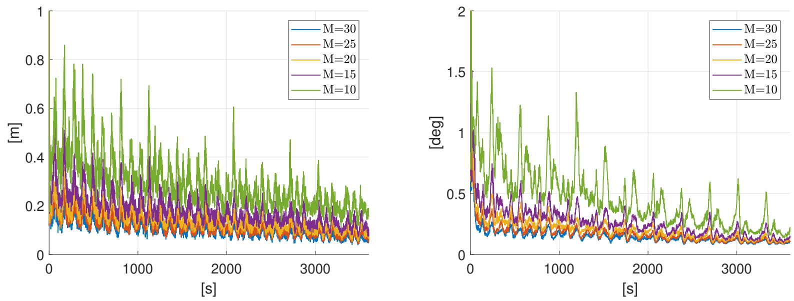

(a) Average relative position error.

(b) Average relative attitude error.

Figure 16: Feature points sensitivity analysis.

5.2.8. Number of Feature Points Sensitivity Analysis

Another important aspect to take into account is the number of considered feature points. In this sensitivity analysis, the nominal scenario with fixed initial conditions and tuning, varying the number of known feature points, has been simulated. In particular, a number of feature points M swinging from 10 to 30 has been considered. The noise level is kept at $\sigma_{pix} = 1$. Modifying the number of feature points implies modifying the measurements and therefore the measurement equation in the EKF. Analogously, the trends of the different estimation errors are reported in Figures 16a and 16b.

These plots show how, increasing the number of feature points, the estimate of both relative position and attitude improves. However, for the presented simulation, considering more than 25 feature points, the benefit of adding more features is reduced and, therefore, it may only represent an additional, ineffective computational cost. As general consideration, a higher number of feature points (25-30) is always preferable to improve the overall estimation error (up to 40% with respect to the case of 10 feature points) and also to guarantee robustness against potential outliers. Furthermore, the particular navigation filter formulation, not considering the feature points in the state vectors, limits the increment of the computational effort to a larger observation matrix.

6. Conclusions

The paper presented a set of Guidance, Navigation and Control (GNC) functions to deal with the problem of 6 degrees of freedom (6DOF) rendezvous in multi-body Cislunar environment, proposing guidance strategies, vision-based navigation techniques and control laws for a coupled orbit-attitude rendezvous and docking. Particular focus on the accurate dynamical modeling required to support the GNC design was maintained along the entire discussion, both to show the positive capabilities offered to the rendezvous trajectories design and to stress the limitations of GNC systems based on incorrect dynamical modeling of multi-body Cislunar space.

Absolute and relative orbit and attitude dynamics were presented and discussed. The accuracy of different modelling approaches was compared, showing that a Full Ephemeris Restricted 4-Body Problem (FER4BP) is beneficial for applications in the Earth-Moon system, with the non-negligible effects of the Sun's gravity. A linearized version of the relative dynamics was presented and used for the development of navigation functions, still based on the FER4BP accurate model.

The knowledge of coupled orbit-attitude absolute and relative dynamics in Cislunar space resulted to be fundamental in designing proper GNC functions and in leveraging natural dynamics to help the rendezvous design process. The proximity trajectory design made use of center and unstable modes, existing in multi-body non-Keplerian dynamics, to provide useful features, such as hovering phases and passive stability of the maneuvers, without active GNC effort.

The guidance and control design was based on open-loop guidance at far-range and closed-loop guidance at close-range. Maneuver cost minimization was sought by exploiting the natural dynamics of multi-body Cislunar environment and an energy optimal framework. The development based on 6DOF coupled dynamics allowed a step further with respect to previous research contributions.

Navigation functions were developed within a vision-based only architecture, proving the feasibility of this navigation method when applied to non-Keplerian multi-body orbits. Visual navigation allowed a 6DOF state estimation, which is embedded in the proposed orbit-attitude GNC design, when dealing with closed-loop guidance and control. This implementation allows a broad applicability to different kinds of spacecraft or, possibly, space objects. The available results augmented the set of those existing in literature, proving the performances of a navigation system without the use of any sensor different from the optical ones.

An example rendezvous scenario with a passively cooperative target orbiting on a lunar L2 NRHO was discussed, applying the proposed GNC functions and defining a possible rendezvous strategy with a FER4BP modeling. The latter includes a subdivision into different rendezvous phases, connected by holding points, and a set of rendezvous trajectories that are inherently safe and optimized in terms of required ΔV. Navigation performances and sensitivity analyses are discussed as well on the selected example scenario.

The available results extended those available in literature, often based on classic restricted 3-body formulations. The GNC design exploits a Full Ephemeris Restricted 4-Body Problem, with Solar Radiation Pressure (SRP), to model the coupled translational and rotational dynamics in multi-body Cislunar environment, which is an advance with respect to existing literature. The proposed 6DOF vision-based only navigation architecture was never investigated in previous non-Keplerian multi-body research studies. Moreover, an integrated GNC design for Cislunar rendezvous, which exploits the natural multi-body dynamics to enhance the relative control performances, was not fully explored by other journal articles.

References

[1] K. Yazdi, E. Messerschmid, A lunar exploration architecture using lunar libration point one, Aerospace Science and Technology 12 (3) (2008) 231 – 240. doi:https://doi.org/10.1016/j.ast.2007.06.001.

[2] International Space Exploration Coordination Group. (ISECG), The Global Exploration Roadmap, Tech. rep., ISECG (2018).

[3] R. Whitley, R. Martinez, Options for staging orbits in cislunar space, in: 2016 IEEE Aerospace Conference, Big Sky, Montana, USA, 5-12 March, 2016, pp. 1–9. doi:10.1109/AERO.2016.7500635.

[4] S. Ueda, N. Murakami, Optimum guidance strategy for rendezvous mission in Earth-Moon L2 Halo orbit, in: Proceedings of the 25th International Symposium on Space Flight Dynamics (ISSFD), Munich, Germany, 19-23 October, 2015, pp. 1–14.

[5] M. Mammarella, E. Capello, G. Guglieri, Robust Model Predictive Control for Automated Rendezvous Maneuvers in Near-Earth and Moon Proximity, in: 2018 AIAA SPACE and Astronautics Forum and Exposition, Orlando, Florida, USA, 17-19 September, 2018. doi:10.2514/6.2018-5343.

[6] R. Gerding, Rendezvous equations in the vicinity of the second libration point, Journal of Spacecraft and Rockets 8 (3) (1971) 292–294. doi:10.2514/3.30263.

[7] P. Gurfil, N. Kasdin, Dynamics and control of spacecraft formation flying in three-body trajectories, in: Proceedings of the AIAA Guidance, Navigation, and Control Conference and Exhibit, Montreal, Canada, 6-9 August, 2001, pp. 1–11. doi:10.2514/6.2001-4026.

[8] A. Héritier, K. C. Howell, Dynamical evolution of natural formations in libration point orbits in a multi-body regime, Acta Astronautica 102 (1) (2014) 332–340. doi:10.1016/j.actaastro.2013.10.017.

[9] K. Mand, Rendezvous and proximity operations at the earth-moon l2 lagrange point: Navigation analysis for preliminary trajectory design, Master's thesis, Rice University, Department of Aerospace Engineering, Houston (2014).
URL https://scholarship.rice.edu/handle/1911/88095

[10] J. C. Sanchez, F. Gavilan, R. Vazquez, Chance-constrained model predictive control for near rectilinear halo orbit spacecraft rendezvous, Aerospace

Science and Technology 100 (2020) 105827. doi:https://doi.org/10.1016/j.ast.2020.105827.

[11] C. D'Souza, T. Crain, F. Clark, J. Getchius, Orion cislunar guidance and navigation, in: AIAA Guidance, Navigation and Control Conference and Exhibit, Hilton Head, South Carolina, USA, 20 - 23 August, 2007, pp. 1–21. doi:10.2514/6.2007-6681.

[12] T. R. Kane, E. Marsh, Attitude stability of a symmetric satellite at the equilibrium points in the restricted three-body problem, Celestial mechanics 4 (1) (1971) 78–90. doi:10.1007/BF01230323.

[13] W. Robinson, Attitude stability of a rigid body placed at an equilibrium point in the restricted problem of three bodies, Celestial Mechanics and Dynamical Astronomy 10 (1) (1974) 17–33. doi:10.1007/BF01261876.

[14] D. Guzzetti, K. C. Howell, Natural periodic orbit-attitude behaviors for rigid bodies in three-body periodic orbits, Acta Astronautica 130 (1) (2017) 97–113. doi:10.1016/j.actaastro.2016.06.025.

[15] D. Guzzetti, K. C. Howell, Attitude dynamics in the circular restricted three-body problem, Astrodynamics 2 (2) (2018) 87–119. doi:10.1007/s42064-017-0012-7.

[16] A. Colagrossi, M. Lavagna, Preliminary results on the dynamics of large and flexible space structures in Halo orbits, Acta Astronautica 134 (2017) 355–367. doi:10.1016/j.actaastro.2017.02.020.

[17] L. Bucci, M. Lavagna, D. Guzzetti, K. C. Howell, Periodic orbit-attitude solutions along planar orbits in a perturbed circular restricted three-body problem for the earth-moon system, Acta Astronautica 147 (2018) 152–162. doi:j.actaastro.2018.03.042.

[18] A. Colagrossi, M. Lavagna, Dynamical analysis of rendezvous and docking with very large space infrastructures in non-keplerian orbits, CEAS Space Journal 10 (1) (2018) 87–99. doi:10.1007/s12567-017-0174-4.

[19] V. Pesce, M. F. Haydar, M. Lavagna, M. Lovera, Comparison of filtering techniques for relative attitude estimation of uncooperative space objects, Aerospace Science and Technology 84 (2019) 318 – 328. doi:https://doi.org/10.1016/j.ast.2018.10.031.

[20] L. Zhang, S. Zhang, H. Yang, H. Cai, S. Qian, Relative attitude and position estimation for a tumbling spacecraft, Aerospace Science and Technology 42 (2015) 97–105. doi:10.1016/j.ast.2014.12.025.

[21] V. Pesce, M. Lavagna, R. Bevilacqua, Stereovision-based pose and inertia estimation of unknown and uncooperative space objects, Advances in Space Research 59 (1) (2017) 236–251. doi:10.1016/j.asr.2016.10.002.

[22] V. Pesce, R. Opromolla, S. Sarno, M. Lavagna, M. Grassi, Autonomous relative navigation around uncooperative spacecraft based on a single camera, Aerospace Science and Technology 84 (2019) 1070–1080. doi:10.1016/j.ast.2018.11.042.

[23] S. Muñoz, J. Christian, E. G. Lightsey, Development of an end to end simulation tool for autonomous cislunar navigation, in: AIAA Guidance, Navigation, and Control Conference, Chicago, Illinois, USA, 10 - 13 August, 2009, pp. 1–21. doi:10.2514/6.2009-5995.

[24] A. Colagrossi, M. Lavagna, Cislunar non-keplerian orbits rendezvous & docking: 6DOF guidance and control, in: 69th International Astronautical Congress, Bremen, Germany 1-5 October, 2018, pp. 1–18.
URL http://hdl.handle.net/11311/1067254

[25] G. Q. Xing, S. A. Parvez, Alternate forms of relative attitude kinematics and dynamics equations, in: 2001 Flight Mechanics Symposium, Greenbelt, Maryland, USA, 19-21 June, 2001, pp. 83–97.
URL https://ntrs.nasa.gov/archive/nasa/casi.ntrs.nasa.gov/20010084965.pdf

[26] R. J. Luquette, Nonlinear control design techniques for precision formation flying at lagrange points, Ph.D. thesis, University of Maryland, College Park (2006).
URL https://drum.lib.umd.edu/handle/1903/4130

[27] L. Bucci, A. Colagrossi, M. Lavagna, Rendezvous in Lunar Near Rectilinear Halo Orbits, Advances in Astronautics Science and Technology 1 (2018) 39–43. doi:10.1007/s42423-018-0012-6.

[28] A. Colagrossi, Absolute and relative 6dof dynamics, guidance and control for large space structures in cislunar environment, Ph.D. thesis, Politecnico di Milano (2019).
URL http://hdl.handle.net/10589/144662

[29] N. Murakami, S. Ueda, T. Ikenaga, M. Maeda, T. Yamamoto, H. Ikeda, Practical rendezvous scenario for transportation missions to cis-lunar station in Earth–Moon L2 Halo orbit, in: Proceedings of the 25th International Symposium on Space Flight Dynamics (ISSFD), Munich, Germany, 19-23 October, 2015, pp. 1–12.

[30] L. Bucci, Mission analysis and operational aspects for a lunar exploration architecture, Ph.D. thesis, Politecnico di Milano (2020).
URL http://hdl.handle.net/10589/153059

[31] G. Gómez, J. Llibre, R. Martínez, C. Simó, Dynamics and mission design near Libration points, Vol. 1, World Scientific, 2001. doi:10.1142/4402.

[32] L. Bucci, M. Lavagna, F. Renk, Phasing and rendezvous operations on non-Keplerian orbits in the Earth-Moon system, in: 69th International Astronautical Congress, Bremen, Germany 1-5 October, 2018, pp. 1–12.
URL http://hdl.handle.net/11311/1067249

[33] L. Bucci, M. Lavagna, F. Renk, Relative dynamics analysis and rendezvous techniques for lunar Near Rectilinear Halo Orbits, in: 68th International Astronautical Congress, Adelaide, Australia, 25-29 September, 2017, pp.

1–9.
URL http://hdl.handle.net/11311/1060479

[34] R. J. Whitley, D. C. Davis, L. M. Burke, B. P. McCarthy, R. J. Power, M. L. McGuire, K. C. Howell, Earth-Moon near rectilinear halo and butterfly orbits for lunar surface exploration, in: AAS/AIAA Astrodynamics Specialists Conference, Snowbird, Utah, USA, 19-23 August, 2018, pp. 1–20.

[35] D. Guzzetti, E. M. Zimovan, K. C. Howell, D. C. Davis, Stationkeeping analysis for spacecraft in lunar near rectilinear halo orbits, in: 27th AAS/AIAA Space Flight Mechanics Meeting, San Antonio, Texas, USA, 5-9 February, 2017, pp. 1–24.

[36] Y. Qi, A. de Ruiter, Station-keeping strategy for real translunar libration point orbits using continuous thrust, Aerospace Science and Technology 94 (2019) 105376. doi:https://doi.org/10.1016/j.ast.2019.105376.

[37] D. Folta, D. Quinn, Lunar frozen orbits, in: AAS/AIAA Space Flight Mechanics Winter Meeting, Galveston, Texas, USA, 27-31 January, 2008, pp. 1–40. doi:10.2514/6.2006-6749.

[38] L. Bucci, M. Lavagna, R. Jehn, et al., Station keeping techniques for Near Rectilinear Orbits in the Earth-Moon system, in: 10th International ESA Conference on Guidance, Navigation & Control Systems (GNC 2017), Salzburg, Austria, 29 May - 2 June, 2017, pp. 1–17.
URL http://hdl.handle.net/11311/1047206

[39] P. K. Seidelmann, L. E. Doggett, P. M. Janiczek, Algorithms, calculators, and computers for celestial navigation, Proceedings of the IEEE 71 (10) (1983) 1201–1204. doi:10.1109/PROC.1983.12749.

[40] F. Colombi, A. Colagrossi, M. Lavagna, Characterization of 6DOF Natural and Controlled Relative Dynamics in Cislunar Space, Acta Astronau-

tica Online First. doi:https://doi.org/10.1016/j.actaastro.2021.01.017.

[41] K. Hill, G. Born, Autonomous interplanetary orbit determination using satellite-to-satellite tracking, Journal of guidance, control, and dynamics 30 (3) (2007) 679–686. doi:10.2514/1.24574.

[42] T. Svoboda, T. Pajdla, V. Hlaváč, Epipolar geometry for panoramic cameras, in: European Conference on Computer Vision, Freiburg, Germany, 2-6 June, 1998, pp. 218–231.
URL https://link.springer.com/content/pdf/10.1007/BFb0055669.pdf

[43] Y. Wang, H. Ji, Integrated relative position and attitude control for spacecraft rendezvous with iss and finite-time convergence, Aerospace Science and Technology 85 (2019) 234 – 245. doi:https://doi.org/10.1016/j.ast.2018.12.005.

[44] J. Zhang, J. D. Biggs, D. Ye, Z. Sun, Finite-time attitude set-point tracking for thrust-vectoring spacecraft rendezvous, Aerospace Science and Technology 96 (2020) 105588. doi:https://doi.org/10.1016/j.ast.2019.105588.

[45] A. Colagrossi, M. Lavagna, Dynamics and control of modular and extended space structures in cislunar environment, in: 26th International Symposium on Space Flight Dynamics (ISSFD), Matsuyama, Japan, 6-9 June 2017, 2017, pp. 1–10.
URL http://hdl.handle.net/11311/1047100

[46] M. Chory, D. Hoffman, J. LeMay, Satellite autonomous navigation - status and history, in: PLANS'86-Position Location and Navigation Symposium, Las Vegas, NV, November 4-7, 1986, pp. 110–121.
URL https://ui.adsabs.harvard.edu/abs/1986pln..symp..110C/abstract

[47] K. D. Hicks, W. E. Iesel, Autonomous orbit determination system for earth satellites, Journal of guidance, control, and dynamics 15 (3) (1992) 562–566. doi:10.2514/3.20876.

[48] H. Jung, M. L. Psiaki, Tests of magnetometer/sun-sensor orbit determination using flight data, Journal of Guidance, Control, and Dynamics 25 (3) (2002) 582–590. doi:10.2514/2.4920.

[49] S. I. Sheikh, D. J. Pines, P. S. Ray, K. S. Wood, M. N. Lovellette, M. T. Wolff, Spacecraft navigation using x-ray pulsars, Journal of Guidance, Control, and Dynamics 29 (1) (2006) 49–63. doi:10.2514/1.13331.

[50] F. Markley, Autonomous navigation using landmark and intersatellite data, in: AAS/AIAA Astrodynamics Conference, Kalispell, Montana, USA, 10-13 August, 1987, pp. 1–12. doi:10.2514/6.1984-1987.

[51] J. Yim, J. Crassidis, J. Junkins, Autonomous orbit navigation of interplanetary spacecraft, in: AAS/AIAA Astrodynamics Specialist Conference, Denver, Colorado, USA, 14-17 August, 2000, pp. 1–11. doi:10.2514/6.2000-3936.